

# EVALUATION OF SAFETY DISTANCES FOR STORAGE OF EXPLOSIVE MATERIALS USING A COMBINATION OF THERMOCHEMICAL COMPUTATIONS AND CFD

HANNIBAL E. FOSSUM<sup>1</sup>, ANDREAS N. OSNES<sup>2</sup> AND  
TOR E. KRISTENSEN<sup>1</sup>

<sup>1</sup>Norwegian Defence Research Establishment (FFI)  
P. O. Box 25, 2027 Kjeller, Norway  
e-mail (corresponding author): hannibal.fossum@ffi.no

<sup>2</sup> Department of Technology Systems, University of Oslo  
P. O. Box 70, 2027 Kjeller, Norway

**Key words:** TNT equivalency, detonation, explosives

**Abstract.** A novel approach to calculating TNT equivalencies and safety distances for explosives, using a combination of thermochemical computations and computational fluid dynamics, is presented. This enables the estimation of safety distances for specific explosives and charge geometries based on physical principles rather than empirical parametrizations. The methodology inherently allows for the simulation of subsequent shock propagation and interaction with surrounding structures, following the detonation of an explosive. Presented results include examples of computed TNT equivalencies for selected commercial explosives, as well as simulated pressure distributions around a detonating stack of dynamite.

## 1 Introduction

Globally, billions of kilograms of commercial explosives are used annually for purposes such as mining, quarrying, construction work, demolitions and weaponry. The manufacturing, transportation and storage of such materials pose considerable safety risks. Two aspects central to safe storage of explosive materials are investigated in this work by combining thermochemical computations and computational fluid dynamics (CFD).

The first part of this investigation details a novel approach for the establishment of robust TNT equivalency values in air for detonating explosives, including both pure substances or mixtures of several compounds (both being referred to herein simply as an *explosive*). The determination of reliable TNT equivalencies is essential for any realistic comparison of explosive materials with regards to evaluation of safety distances.

The concept of TNT equivalency is confusing because it may relate to various facets of relative explosive output [1, 2]. Firstly, the term can refer to a unit of energy, defined by convention and used typically to express the power of nuclear weapons or cosmic events. Secondly, it can be a relative measure for air blast phenomena (overpressure or impulse). Thirdly, TNT equivalency is often used rather arbitrarily as a relative effectiveness factor, in terms of “demolition power”, for comparison of explosives. Unfortunately, the second and third aspects are regularly mixed up.

It is the second aspect above that is relevant for evaluation of safety distances, in this context being defined as the amount of TNT (in pure form and shaped as a hemisphere) which, during detonation on the ground level and at a precise distance, yields the same blast overpressure or blast impulse as the mass unit of the considered explosive. Although strictly defined, TNT equivalencies for different explosives have traditionally been derived by simply comparing an easily obtained attribute of the performance of the explosive in question to that for TNT, e.g. directly relating the heats of detonations or the total energies of detonations.

In this work, more realistic TNT equivalencies are derived by carrying out one-dimensional gas-dynamic simulations of spherical-charge detonations (in air) for various explosives. The simulations are compared to corresponding simulations of TNT. This results in TNT equivalencies, either by peak overpressures or impulses, that are applicable for evaluation of the safety distances relevant to storage of explosives. The material properties and detonation parameters for specific explosives are obtained using a thermochemical code.

The second part of the study regards the detonation of pallets loaded with stacked cardboard boxes holding dynamite, this being the conventional way of storing such cartridge explosives. Gas-dynamic simulations are used to map peak pressures in the volume surrounding detonating stacks for different initiation scenarios. Geometrical effects, e.g. from corners, have large effects on the pressure distributions in the near-field of the detonation. These effects can possibly be exploited to improve safety or efficiency in storage facilities containing such palletted stacks.

The method detailed herein enables the estimation of safety distances for specific explosives and charge geometries based on physical principles rather than empirical parametrizations. Furthermore, the methodology inherently allows for the simulation of subsequent shock propagation and interaction with surrounding structures, following the detonation of an explosive.

This paper is structured as follows: Section 2 provides an overview of the thermochemical computations, the gas-dynamic simulation framework and the computational setup. Section 3 contains the simulation results. The results from the one-dimensional computations are presented first, followed by the simulations of dynamite stack detonations. Finally, concluding remarks are contained in section 4.

## 2 Method

### 2.1 General procedure

The simulations in this study have been performed via a two-step approach.

Firstly, a thermochemical code, EXPLO5 [3, 4], is used to compute material properties and detonation parameters for a specified explosive.

Secondly, the gas dynamics of the detonating explosive is simulated in a shock-capturing compressible-fluid flow solver, CharLES [5, 6]. Output from EXPLO5 is used to define the material properties of the explosive, as well as the initial conditions, in CharLES.

The output from the second step is a time-dependent, three-dimensional flow field describing the detonation by means of pressure, density and velocity fields. These data are post-processed in order to extract useful information, such as pressure levels at selected distances from the detonating explosive.

### 2.2 Thermochemical solution

EXPLO5, v6.03, is a thermochemical code that can estimate, among others, the equilibrium composition and thermodynamic parameters of state of detonation products along the shock adiabat of the detonation products for ideal detonations. The program contains a precompiled database with hundreds of chemical reactants and products with associated enthalpies of formation.

The detonation parameters are calculated based on a chemical-equilibrium, steady-state detonation model. The equilibrium composition of detonation products is calculated by applying the free-energy minimization technique of Dantzig, Johnson and White [7], giving a set of equations solved iteratively by a modified Newton-Raphson method.

The state of detonation products can be described by various equations of state (EOS), such as the Becker-Kistiakowsky-Wilson (BKW) EOS or the Jacobs-Cowperthwaite-Zwisler (JCZ3) EOS for gaseous products. The thermodynamic functions of the products are derived using the BKW EOS (for gases) or the Murnaghan EOS (for condensed products).

The thermochemical calculations assume that the detonation is well represented by a Chapman-Jouget (CJ) detonation. The CJ point is computed by numerical determination of the minimum value of the detonation velocity along the shock adiabat of the detonation products. Detonation parameters (pressure, velocity, heat, etc.) at the CJ point is found from the EOS for the products.

From the CJ point, the isentropic expansion of the products is calculated (by numerical integration), and non-linear curve-fitting [8] yields coefficients for the Jones-Wilkins-Lee (JWL) EOS. The JWL EOS enables the calculation of the released detonation energy which will be available to perform mechanical work. Highly resolved density domains were used both in the calculations of the detonation-products adiabat and the JWL coefficients.

The relevant parameters from EXPLO5 for subsequent gas-dynamics simulations are the JWL coefficients, the detonation velocity, and the released detonation energy.

### 2.3 Gas-dynamic solution

The motion of the gas phases are governed by the compressible Navier-Stokes equations. However, the equations of state describing the detonation-product gases and the ambient air are very different, and thus a multi-component model is required. Allaire's five equation model [9] is used for this purpose, with viscous terms included.

In index notation, with summation on double indices and  $i \in \{1, 2, 3\}$ , the governing equations can be written

$$\frac{\partial \rho_1 z_1}{\partial t} + \frac{\partial \rho_1 z_1 u_i}{\partial x_i} = 0, \quad (1)$$

$$\frac{\partial \rho_2 z_2}{\partial t} + \frac{\partial \rho_2 z_2 u_i}{\partial x_i} = 0, \quad (2)$$

$$\frac{\partial z_1}{\partial t} + u_j \frac{\partial z_1}{\partial x_j} = 0, \quad (3)$$

$$\frac{\partial \rho u_i}{\partial t} + \frac{\partial (\rho u_i u_j + p)}{\partial x_j} = \frac{\partial \tau_{ij}}{\partial x_j}, \quad (4)$$

$$\frac{\partial (\rho e + \frac{1}{2} \rho u_i u_i)}{\partial t} + \frac{\partial (\rho e u_j + \frac{1}{2} \rho u_i u_i u_j + u_j p)}{\partial x_j} = \frac{\partial (u_i \tau_{ij} - q_j)}{\partial x_j}, \quad (5)$$

where  $\rho_k$  and  $z_k = z_k(\mathbf{x}, t)$  are the phase-specific mass density and the volume fraction of component  $k$ , respectively.  $u_i = u_i(\mathbf{x}, t)$  is the velocity in the  $i$ 'th direction,  $p = p(\mathbf{x}, t)$  is the static pressure,  $\tau_{ij} = \tau_{ij}(\mathbf{x}, t) = \mu \left( \frac{\partial u_i}{\partial x_j} + \frac{\partial u_j}{\partial x_i} \right) - \frac{2\mu}{3} \delta_{ij} \frac{\partial u_i}{\partial x_i}$  is the viscous stress tensor,  $e = e(\mathbf{x}, t)$  is the specific internal energy and  $q = q(\mathbf{x}, t) = \lambda \partial T / \partial x_j$  is the heat flux, where  $\lambda$  is the heat conductivity. Viscosity is assumed to vary with temperature as a power law, so that  $\mu = \mu_0 (T/T_0)^{0.76}$ , where  $\mu_0$  and  $T_0$  are the kinematic viscosity and temperature at reference conditions. A constant Prandtl number of 0.7 relates the thermal conductivity and viscosity. The position vector is defined by  $\mathbf{x} = x_i = (x, y, z)$ .

Additionally, an equation of state is required for each gas component. In the current work, the Jones-Wilkins-Lee (JWL) equation of state (EOS) and the ideal gas EOS are used to model detonation gases and air, respectively.

The multi-component model described by (1)–(5) is implemented in the compressible fluid solver, resulting in a modified version of CharLES. In CharLES, the numerical method used for the gas phase is a finite-volume method with low dissipation and dispersion, developed for Large Eddy Simulations on unstructured grids [5]. The Harten-Lax-van Leer-Contact (HLLC) Riemann solver [10] is used to compute fluxes between neighbouring

cells, and the solution is advanced in time by a third order explicit Runge-Kutta scheme. The solver is highly parallelized.

For the one-dimensional simulations of spherical detonations, the face values are reconstructed using an Essentially Non-Oscillatory (ENO)-scheme to ensure sharp resolution of shocks. With the present implementation of the multi-component model, this scheme is not robust enough for general three-dimensional simulations. Therefore, a simpler first-order reconstruction of face values are used instead in this case.

### 2.3.1 Initial conditions from a similarity solution

For the spherical-detonation simulations, it is assumed that the detonation of the explosive is adequately described as a CJ detonation. The chemical reactions are assumed to occur within an infinitely thin layer immediately behind the shock front, and this layer terminates at the CJ point. The flow behind this point is assumed to be described by a similarity solution.

The similarity solution is described in e.g. [11]. Some of the results are repeated here for completeness. The basic assumptions required of this model are as follows:

- The flow is one-dimensional and self-similar.
- The adiabatic index (heat capacity ratio) of the detonation products is constant.

The latter assumption can be avoided, e.g., by using the phase-plane method of Kuhl [12]. However, the differences in density, pressure and velocity profiles between these methods are roughly between 1 and 2 % [12].

With these assumptions, the solution of the gas-dynamic equations is given in terms of a chosen set of similarity variables. Let  $\xi = r(Dt)^{-1}$  where  $r$  is the radial coordinate,  $D$  is the detonation velocity and  $t$  is time,  $\phi(\xi) = u/D$ , where  $u$  is the gas velocity,  $\eta(\xi) = c/D$ , where  $c$  is the speed of sound. Then the steady flow solution is given by:

$$\phi' = \left( \frac{j\phi}{\xi} \right) \frac{\eta^2}{(\phi - \xi) - \eta^2}, \quad (6)$$

$$\eta' = - \left( \frac{\gamma - 1}{2} \right) \left( \frac{j\eta\phi}{\xi} \right) \frac{\phi - \xi}{(\phi - \xi)^2 - \eta^2}, \quad (7)$$

where  $j = 0, 1, 2$  corresponds to planar, cylindrical and spherical geometry respectively, and  $\gamma$  is the adiabatic index. These equations can be integrated from the CJ-point, where  $\xi = 1$ ,  $\phi = \phi_1$  and  $\eta = \eta_1$ . For  $j = 1$  or  $j = 2$  the equations are singular at the front, and the solution in the immediate proximity of this point is instead computed by the first-order series expansion:

$$\phi(\xi) = \phi_1 - \sqrt{\frac{2j\phi_1\eta_1}{\gamma + 1}} (1 - \xi)^{1/2} + \dots, \quad (8)$$

$$\eta(\xi) = \eta_1 - \frac{\gamma - 1}{2} \sqrt{\frac{2j\phi_1\eta_1}{\gamma + 1}} (1 - \xi)^{1/2} + \dots \quad (9)$$

The series expansion is used to compute a single point behind the CJ point, and the rest of the profile follows by integration of equations 6 and 7. Since the expansion behind the CJ point is isentropic, pressure and density profiles are found by

$$p(\xi) = p(1) \left( \frac{\eta(\xi)}{\eta(1)} \right)^{2\gamma/(\gamma-1)}, \quad (10)$$

$$\rho(\xi) = \rho(1) \left( \frac{\eta(\xi)}{\eta(1)} \right)^{2/(\gamma-1)}. \quad (11)$$

### 2.3.2 Initial conditions from programmed burn

The evolution of a general detonation front in an explosive with complex charge geometry is difficult to compute accurately. Direct numerical simulations are infeasible, due to the conflicting requirements of high resolution of the reaction zone and the large amounts of explosives. Thus, programmed burn has emerged as an engineering solution. The programmed-burn approach has been shown to produce acceptable results without large computational cost [13, 14].

Based on the results from the thermochemical code, the detonation velocity is prescribed throughout the explosive. With this procedure, virtually no computational effort is spent on the detonation front and reaction zone calculations per se. Only the rest of the gas-dynamics problem, where the detonation energy performs mechanical work, is simulated directly.

In the present implementation, the programmed burn model is defined simply by a scalar field representing a local initiation time,

$$t_{\text{init}}(\mathbf{x}) = d_I/D.$$

Here,  $d_I = d_I(\mathbf{x})$  is the distance to the closest detonation initiation point. Once the simulation time reaches  $t_{\text{init}}$  for a given computational cell, the appropriate detonation energy (given by the thermochemical code) is released at that location.

## 3 Results

### 3.1 Spherical detonations

For the free-space spherical detonations, several common commercial explosives have been simulated. Selected coefficients for the JWL EOS for each (fully reacted) explosive are listed in Table 1, as are the detonation velocities and detonation-energy releases calculated in the thermochemical solver. Only parameters relevant to the gas-dynamics simulations are shown.

Table 1: Selected detonation parameters from the thermochemical code<sup>I</sup>; JWL constants ( $A$ ,  $B$ ,  $R_1$ ,  $R_2$ , and  $\omega$ ), detonation velocity ( $D$ ), and detonation energy ( $E_D$ ) are shown.

Explosive	$A$ [GPa]	$B$ [GPa]	$R_1$	$R_2$	$\omega$	$D$ [m/s]	$E_D$ [kJ/cm <sup>3</sup> ]
TNT	698.754	20.9134	5.30235	1.69442	0.425571	7158.2	7.1229
EGDN	635.736	16.3697	5.20740	1.47310	0.312138	7519.3	10.2795
HMX	1200.182	41.8148	5.14251	1.70474	0.516399	9194.8	11.2751
Nitroglycerine	802.456	19.4111	5.29319	1.51644	0.343281	7786.9	10.1127
PETN	812.029	24.8674	4.90760	1.53975	0.431519	8423.4	10.8304
Picric acid	789.910	23.2665	5.14538	1.67083	0.463379	7628.2	7.7859
RDX	906.164	31.5984	4.88605	1.60997	0.497743	8881.3	10.7488
Tetryl	743.711	24.1145	5.03631	1.61632	0.464622	7871.2	8.5857
AN	102.441	2.4722	5.65876	1.85368	0.390625	3723.5	1.5584
( $\rho = 800$ kg/m <sup>3</sup> )							
ANFO	94.244	3.2328	4.99013	1.42873	0.347341	4790.5	3.4817
( $\rho = 800$ kg/m <sup>3</sup> )							
Blasting gelatin	629.476	15.9885	5.21995	1.47715	0.316859	7408.6	9.8517
Comp. A-3	1139.844	34.2849	5.53357	1.71944	0.483375	8429.8	9.1571
Comp. B	867.256	28.3582	5.19281	1.65308	0.475931	8122.7	8.9343
Comp. C-4	1121.466	34.4409	5.47924	1.71300	0.488059	8455.1	9.2536
Octol 75-25	1072.979	34.6360	5.20599	1.66865	0.501066	8665.9	10.0424
Pentolite 50-50	657.216	23.8726	4.95074	1.59822	0.467663	7754.1	8.5708

<sup>I</sup> The EXPLO5 density increase ratio was set to 1.005 for the calculation of the shock adiabat of the products, and the density decrease ratio was set to 1.01 for the calculation of the expansion isentrope of the products (with a freeze temperature of 1800 K). Only formation of solid carbon as graphite (i.e., not diamond) was allowed in the EXPLO5 calculations. All explosives have densities close to their theoretical maximum densities unless otherwise noted.

For the gas-dynamics simulations, a series of expanding one-dimensional computational grids have been used, in which consecutive cell widths (and hence also cell volumes) expand in the  $x$ -direction, as shown in Figure 1. Cell widths in both  $y$ - and  $z$ -direction expand (corresponding to the two angular directions) with increasing  $x$ , though only one direction is visible in the figure. Using multiple meshes is significantly more efficient than using a single mesh for the entire simulation. Interpolation between meshes introduces a small error that a single mesh would avoid. However, that error was found to be insignificant for the current simulations.

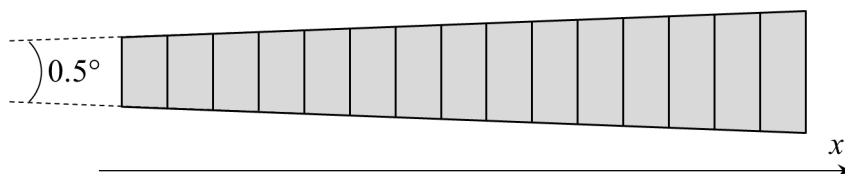


Figure 1: Schematic illustration of the one-dimensional mesh used in the spherical-detonation simulations.

The initial mesh represents a  $0.5^\circ$  spherical sector from  $x = 0.01R$  to  $x = 2R$ , where  $R = (3M/4\rho\pi)^{1/3}$ . Note that  $R$  is simply the radius of the explosive charge, based on  $M$ , the total mass of explosive (typically 1 kg in the present simulations), and  $\rho$ , the density of the explosive material. Once the shock wave reaches  $x = 0.85R$  in the initial mesh, the simulation data is interpolated to a new mesh with twice the resolution and domain size, and the simulation is continued. This interpolation procedure is repeated iteratively on successively coarser meshes until a desired distance (or time) of shock propagation has been calculated.

All the successive one-dimensional meshes comprise 1188 computational cells and use a spherical sector of  $0.5^\circ$  (in both angular directions). The meshes are uniformly spaced in the  $x$ -direction. The time-steps are determined based on a constant CFL number of 0.5, based on the cell width in the  $x$ -direction.

From the results of the simulated detonations, TNT equivalencies can be calculated as follows. The recorded shock pressure and impulse of the positive phase are recorded for all locations within  $5 \leq Z \leq 40$ . Then, these results are compared to a similar simulation of TNT. Since the results are a function of the scaled distance,  $Z = x/\sqrt[3]{M}$ , the TNT mass can be scaled so that the pressure or impulse at a certain (unscaled) distance matches for both explosives. The TNT equivalency is the ratio of the mass of the matching TNT charge to the mass of the other explosive. The TNT equivalency computed in this way is generally a function of scaled distance. The results of the calculations are listed in Table 2.

From a practical point of view, the TNT equivalency values in Table 2 for ammonium nitrate (AN) and ammonium nitrate/fuel oil (ANFO) hold particular importance with



Table 2: TNT equivalencies for selected commercial explosives, as computed with the two-step procedure. As the results did not depend significantly on distance,  $Z$ , only the average TNT equivalency is reported for each explosive.

Explosive	TNT equivalency by impulse	TNT equivalency by peak overpressure
TNT	1	1
EGDN	1.88	1.38
HMX	1.83	1.37
Nitroglycerine	1.71	1.31
PETN	1.76	1.34
Picric acid	1.09	1.05
RDX	1.79	1.35
Tetryl	1.31	1.15
AN ( $\rho = 800 \text{ kg/m}^3$ )	0.20	0.42
ANFO ( $\rho = 800 \text{ kg/m}^3$ )	0.69	0.80
Blasting gelatin	1.74	1.32
Comp. A-3	1.43	1.20
Comp. B	1.42	1.20
Comp. C-4	1.46	1.22
Octol 75-25	1.61	1.28
Pentolite 50-50	1.34	1.17

regard to explosives safety due to the enormous quantities of these materials being stored and transported at any time. For AN, which is by far the most important constituent of most civilian explosives, the TNT equivalency depends heavily on the choice of overpressure or impulse as the determining air-blast parameter. This may partly explain the difficulties associated with the establishment of robust equivalency values for this particular explosive.

In addition to the values in Table 2, we have also calculated the corresponding TNT equivalencies for a number of emulsion-matrix compositions (the non-sensitized precursor to emulsion explosives) obtained from a number of major producers of civilian explosives. All of these have TNT equivalencies, according to the method reported here, in the range of roughly 0.80 by overpressure and between approximately 0.65 and 0.70 by impulse.

When comparing the simulated pressure field for TNT to experimental data, shown in Figure 2, the results show good agreement; the underprediction of the simulated detonation pressure (between 20 % and 35 %) is acceptable given the wide pressure range (three orders of magnitude), and the results are in line with previously published simulation data [15]. The evolution of the pressure field with distance matches the experiment very well.

The peak pressure is underpredicted partly due to the finite size of the control volumes used in these simulations. However, since that effect will similarly reduce peak pressures for all explosives, it is not likely to have much impact on TNT equivalencies.

The results presented in the above is indicative of both the quality and usefulness of the two-step approach. In the following, an analogous procedure is applied to simulate detonations in more complicated cases, thereby assessing required safety distances for storage of explosive materials.

### 3.2 Detonating stacks of dynamite

Most calculations of detonation pressures, and hence related safety distances, are based on spherical detonations and TNT equivalencies. With the approach outlined in previous sections, case-specific calculations can be performed, allowing more accurate estimates of realistic pressure fields.

In the following, detonations of a stack of dynamite are simulated, with different points and planes of initiation. The particular dynamite formulation used in this study has been obtained from a leading European manufacturer. The composition contains ammonium nitrate (AN), ethylene glycol dinitrate (EGDN), nitrocellulose (NC) and various additives.

The simulation domain is illustrated in Figure 3a; the geometry represents a stack on a standard Euro-pallet (EUR 1; 1.2 by 0.8 m<sup>2</sup>) sitting on the ground, loaded with 1,000 kg of cartridge dynamite, contained in five layers of cardboard boxes. The pallet itself is 0.144 m tall, and the height of the stack of dynamite is 1.4 m. The ground surface is included as a fully shock-reflecting surface in the simulations, whereas the materials of the pallet and stack are not.

The coordinate system of the computational domain is defined such that the longer

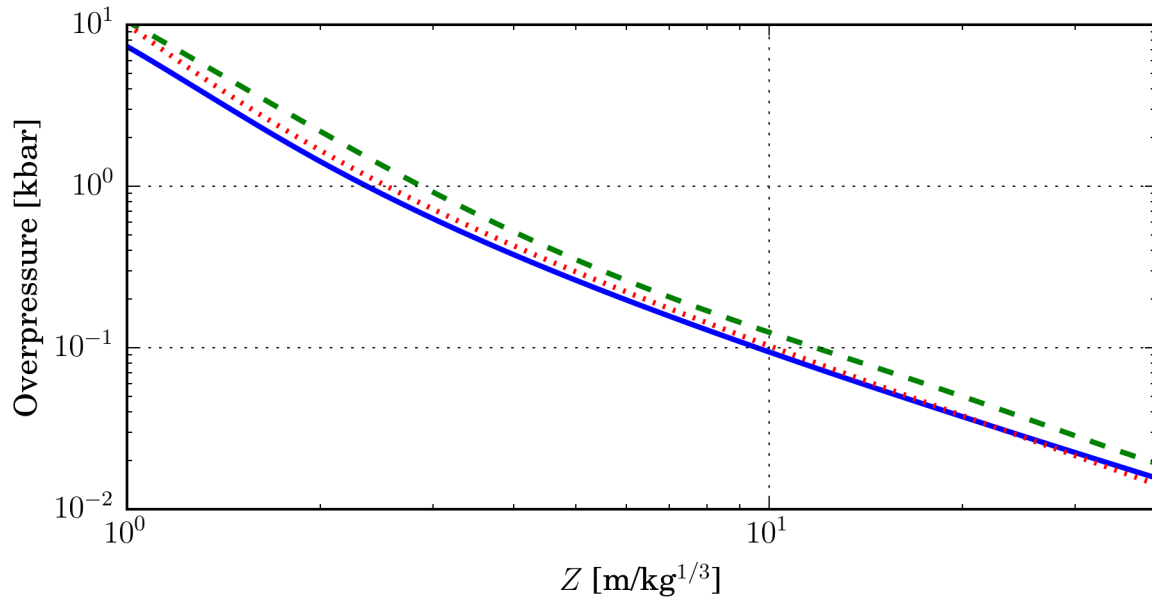
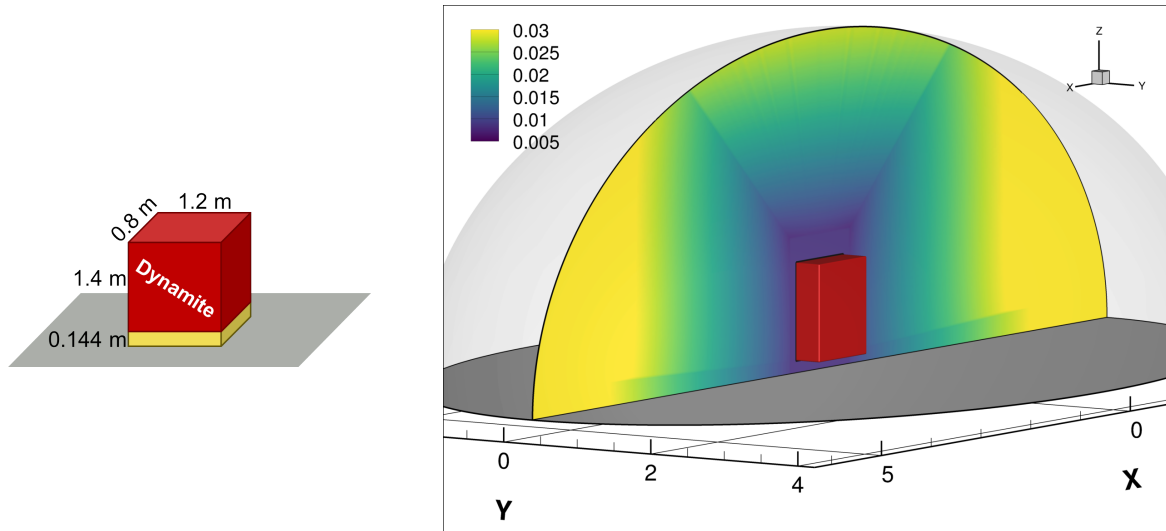


Figure 2: TNT-detonation pressure data from the present simulations (—), the experimental data compiled by Kingery and Bulmesh [16] (---), and the numerical simulation of Grisaro [15] (·····).



(a) Schematic illustration of the pallet and stack geometry.

(b) Computational domain, with a cutplane at  $y = 0$ , colored by the cubic root of local cell volume. The stack of dynamite is marked in red.

Figure 3: The geometry (left) and computational domain (right) of the detonating-dynamite simulations.

edge of the pallet (1.2 m in length) runs along the  $x$ -direction, and  $z$  is the vertical coordinate. In the following, the *left* side of the stack detonates the side that is parallel to the  $y$ -axis and placed at the negative  $x$ -value. The *back* side of the stack detonates the side that is parallel to the  $x$ -axis and placed at the negative  $y$ -value. The *right* and *front* sides are defined analogously (and with opposite signs of the left and back side positions, respectively).

The computational domain is shown in Figure 3b, where the mesh resolution is also indicated; the cutplane at  $y = 0$  (through the middle of the stack) is colored by the cubic root of the local cell volume, i.e. an estimate of a typical local edge length for a computational cell. The smallest edge in the mesh, inside the explosive (i.e. inside the stack of dynamite) is 8.33 mm, whereas the largest edge, at the outer boundary, is 56.4 mm. The total number of computational cells is 25,666,560. Case L3 has a different resolution, to be discussed.

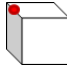
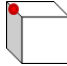
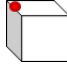
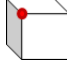
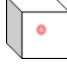
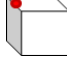
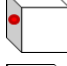
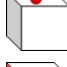
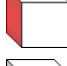

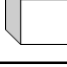
Given the three-dimensional nature of the problem, the mesh must also be three-dimensional. To allow reasonable computation times, the mesh resolution will be significantly reduced compared to the one-dimensional cases of Section 3.1, but the reduction in mesh density is somewhat mitigated by using a non-uniform mesh; as shown in Figure 3b, the mesh is most finely resolved in and near the explosive, where the peak pressures are highest.

All simulations, except L3, used a computational time step of  $\Delta t = 0.12 \mu\text{s}$ . 15,000 time steps were simulated, giving a total simulation time of 1.8 ms. Each simulation

required roughly 3,200 CPU-hours to complete.

Table 3 lists the 14 cases simulated. The simulations are divided into three case series; K, L, and M. The rationale and results for each of the series are discussed in the following.

Table 3: Overview of simulation cases and their initiation locations. Case L3 (\*) is a high-resolution ENO-reconstruction version of case K2.

Case	Initiation location	Illustration
K1	Point, center of upper-left edge	
K2	Point, center of upper-left edge	
K3	Point, center of upper-left edge	
L1	Point, upper-front-left corner	
L2	Point, centroid of stack	
L3*	Point, center of upper-left edge	
L4	Point, center of left side	
L5	Point, center of top side	
M1	Plane, left side	
M2	Plane, front side	
M3	Plane, top side	

### 3.2.1 Case series K: Worst-case pressure field

The cases in series K are simulated to determine the appropriate choice of density for the explosive material. Whereas the real density of the simulated dynamite is  $\rho_{\text{real}} = 1,500 \text{ kg/m}^3$ , the stack is not packed 100 % efficiently; only 49.6 % of the stack volume consists of dynamite. It is therefore possible to define a new pseudo-dynamite material with 49.6 % of the real density, i.e. use  $\rho_{\text{pseudo}} = 744 \text{ kg/m}^3$ . The pseudo-material density can be used both in the thermochemical and gas-dynamical simulations (case K1) or only for the gas dynamics (case K3). Alternatively, the real dynamite density can be used

in both steps, accompanied by a reduction in stack volume to account for the packing inefficiency (case K2). All of the K simulations are initiated in a point on the center of one of the upper edges of the stack.

Given the difficulty involved in determining which of the three K simulations represent the most realistic macroscopic model of a stack inefficiently packed with dynamite, the worst case (in terms of maximum pressure values) is used as a basis for the other case series (L and M).

Figure 4 shows the maximum pressure values,  $p_{\max}$  in the  $(x, z)$ -plane (with  $y = 0$ ) for the three cases in series K. In this and following figures,  $p_{\max}$  always refers to the maximum in time and in the vertical direction up to the stack height, i.e.,

$$p_{\max}(x, y) = \max_{t>0 \wedge z<1.544 \text{ m}} p(\mathbf{x}, t). \quad (12)$$

In the specific case of the present simulations,  $p_{\max}$  is an accurate estimate of the maximum of the peak pressure trailing the shock front, also referred to as the shock pressure.

From the data shown in Figure 4, it is clear that case K2 represents the highest maximum-pressure values. Hence, simulating a smaller stack with 100 % packing efficiency is the most conservative model for inefficient packing. For case series L and M, each stack dimension is thus reduced by a factor  $(\rho_{\text{pseudo}}/\rho_{\text{real}})^{1/3}$ , and  $\rho_{\text{real}}$  is used as the density of the explosive. The bottom of the stack remains at  $z = 0.144$  m above ground level and horizontally centered at  $(x, y) = (0, 0)$ .

### 3.2.2 Case series L: Point initiations

In case series L, various point initiations on the stack are considered, specifically in one corner, one of the edge centers, one of the side centers, and the stack centroid. Comparison of these simulations may reveal information about the dependence of the pressure field on initiation-point location. Note that case L3 is merely a high-resolution version of case K2, thereby allowing for an indicative mesh-resolution study, briefly discussed in Appendix A.

Figure 5 shows the maximum pressures,  $p_{\max}$  in the  $(x, z)$ -plane (with  $y = 0$ ) for cases L2, L4 and M1. As expected, the pressure field is symmetric for simulation L2. Within 4 meters from the center of the stack, the maximum pressure falls below 1 kbar. In comparison, case L4 yields higher pressure values on the right side of the stack relative to the left; at 4 m from the stack centroid, the pressure is more than twice as high on the right side. This is consistent with the fact that the rightward detonation propagates through more explosive material.

Another way of comparing the geometric effects of the initiation point on the pressure field is by considering isocurves in the  $xy$ -plane, as shown in Figure 6. The symmetry of case L5 is apparent, as expected. It is also worth noting that the highest pressure values (for a given distance from the stack) are encountered in the  $x$ - and  $y$ -directions

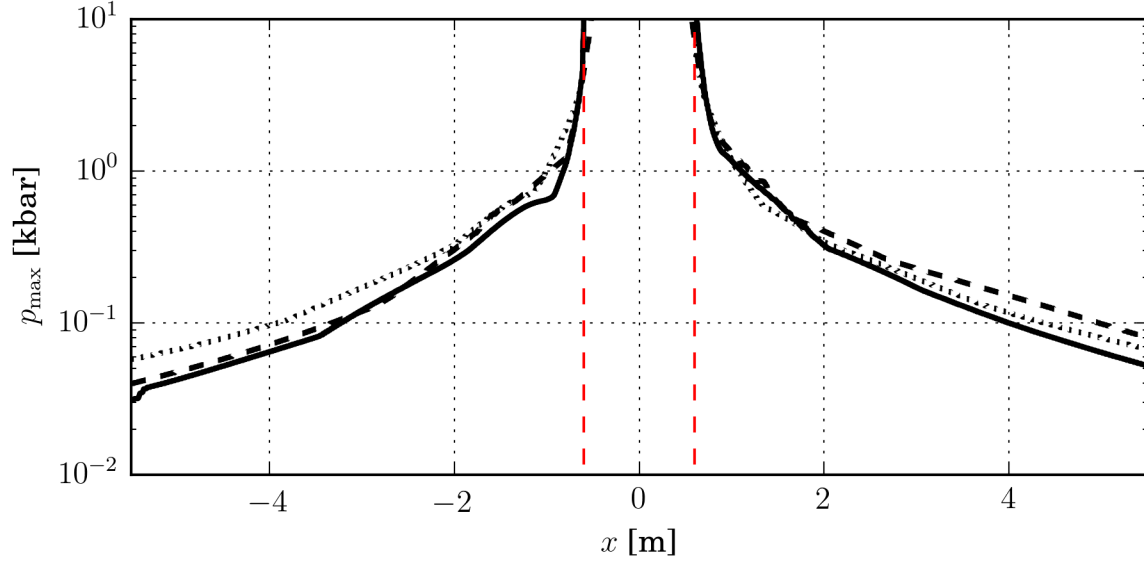


Figure 4: Maximum pressure,  $p_{\max}$ , as a function of  $x$ -distance (with  $y = 0$ ) from the center of the dynamite stack for cases K1 (—), K2 (---), and K3 (·····). The edges of the dynamite stack (real dimensions) are marked by vertical red (dashed) lines.

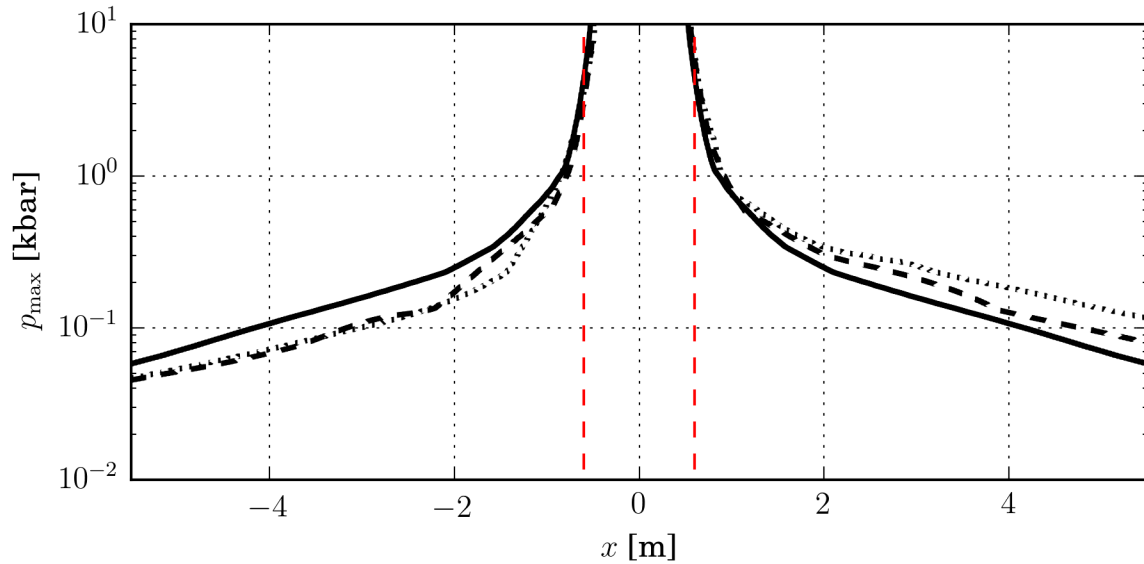


Figure 5: Maximum pressure,  $p_{\max}$ , as a function of  $x$ -distance (with  $y = 0$ ) from the center of the dynamite stack for cases L2 (—), L4 (---), and M1 (·····). The edges of the dynamite stack (real dimensions) are marked by vertical, red (dashed) lines.

(i.e. directly to the front, back, left and right of the stack), even for case L1, which is initiated in the upper-left-front corner.

From Figure 6, it appears that the initiation point is not critical for the evolution of the pressure field, although the effects of altering the initiation point are clearly visible. Case L4 generally seems to produce the smallest values of  $p_{\max}$ , whereas there is no clear “worst-case” for all the horizontal directions considered. Also, given how  $p_{\max}$  is defined, any high-pressure regions above the height of the stack are not accounted for in the data considered here.

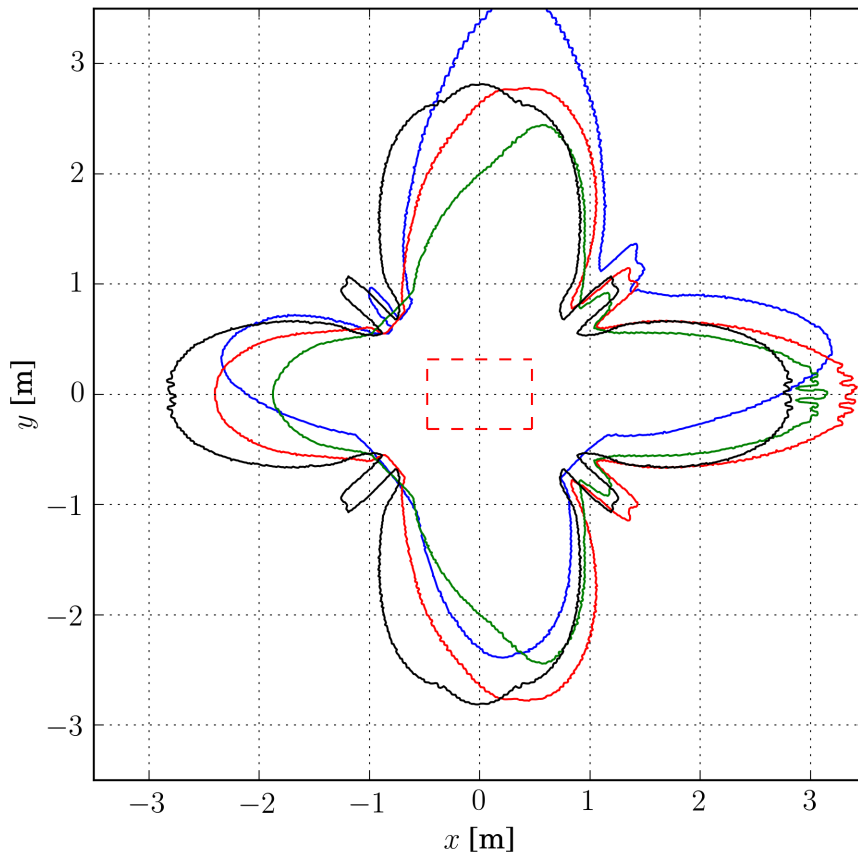


Figure 6: Isocurves in the  $xy$ -plane of  $p_{\max}(x, y) = 0.2$  kbar for cases K2 (red), L1 (blue), L4 (green), and L5 (black). The edges of the dynamite stack (real dimensions) are marked by red, dashed lines.

To obtain more information about the spatial structure of the detonation dynamics, density gradients can be considered. Figure 7 shows a representation of the density-gradient field at simulation time  $t = 0.612$  ms for cases L4 and M1. To improve the



visualization of the gradients, a pseudo-Schlieren technique is used; the shading in Figure 7 indicates the value of

$$F(\rho) = \exp\left(-30\frac{|\nabla\rho|}{|\nabla\rho|_{\max}}\right),$$

in which  $\nabla\rho = \partial\rho/\partial x_i$  is the density gradient, and  $|\nabla\rho|_{\max} = \max_{\text{plane}} |\nabla\rho|$  is the in-plane spatially maximal norm of the density gradient.

From Figure 7, the qualitative features of cases L4 and M1 look generally similar; several triple points can be identified, and a reflecting shock from the ground is seen as a black flattened structure in the lower part of the stack outline in both cases. However, the reflecting shock is more clearly seen in Figure 7b, indicating that the reflected shock is relatively (to the other pressure gradients in the domain) much stronger in case M1 than case L4.

The left part of the shock structure differs in the two cases; the shock front of case M1 is more smooth than that of case L4, which has a visible kink. The kink is a result of geometric effects of the explosive charge, specifically the effect of the upper-left edge of the stack. In the case of M1, the entire left side initiates the detonation, whereas for case L4 only a single point at the left side acts as a trigger. In the latter case, a shock front thus approaches the upper-left edge perpendicularly.

It can also be seen that the detonation front is closely followed by another density gradient, giving the front the appearance of an expanding shell. This second gradient is an inward propagating shock wave caused by overexpansion of the detonation gases. Eventually, that shock wave will implode towards the detonation center and create a secondary outward shock wave.

### 3.2.3 Case series M: Plane initiations

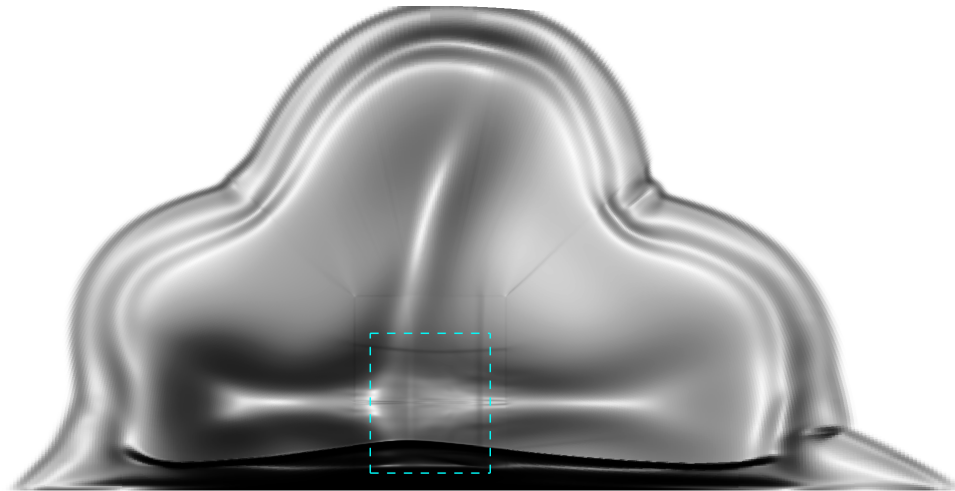
Case series M covers various full-plane initiations. By the symmetry of the problem, the simulations in this case series cover initiations from all possible sides of the stack (except the bottom).

From Figure 5, it is evident that the plane initiation, case M1, yields a higher maximum pressure than the two point initiations. This result also holds when considering all the point-initiation simulations as a whole compared to all the plane-initiation simulations as a whole; the plane initiations represent worst-case scenarios in terms of resulting maximum pressures.

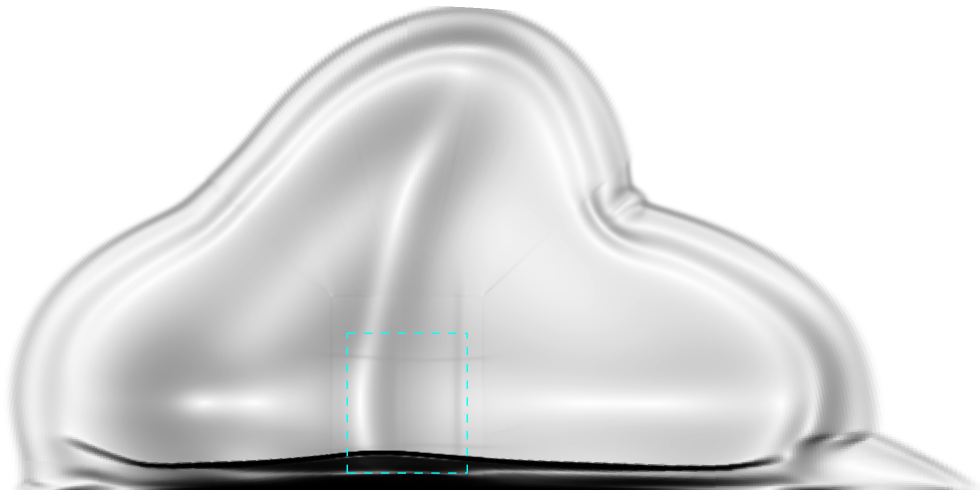
In order to estimate the highest possible peak pressure levels around a stack of dynamite, it is thus sufficient to consider only all possible plane initiations, i.e. cases M1–M3 and their relevant reflections. By accumulating data from all such initiations, a worst-case pressure field can be calculated simply by using the pointwise maximum over all the initiations<sup>1</sup>. Such a worst-case pressure field is shown in Figure 8.

---

<sup>1</sup>Of course, the computed  $p_{\max}$  field for each case is itself a casewise worst case, as defined by Equation (12).



(a) Case L4.



(b) Case M1.

Figure 7: Snapshots at time  $t = 0.612$  ms of the  $xz$ -plane (with  $y = 0$ ), colored by a function of the density gradient,  $F(\rho)$ . Dark shading indicates higher gradients. The edges of the dynamite stack (real dimensions) are marked by blue, dashed lines.

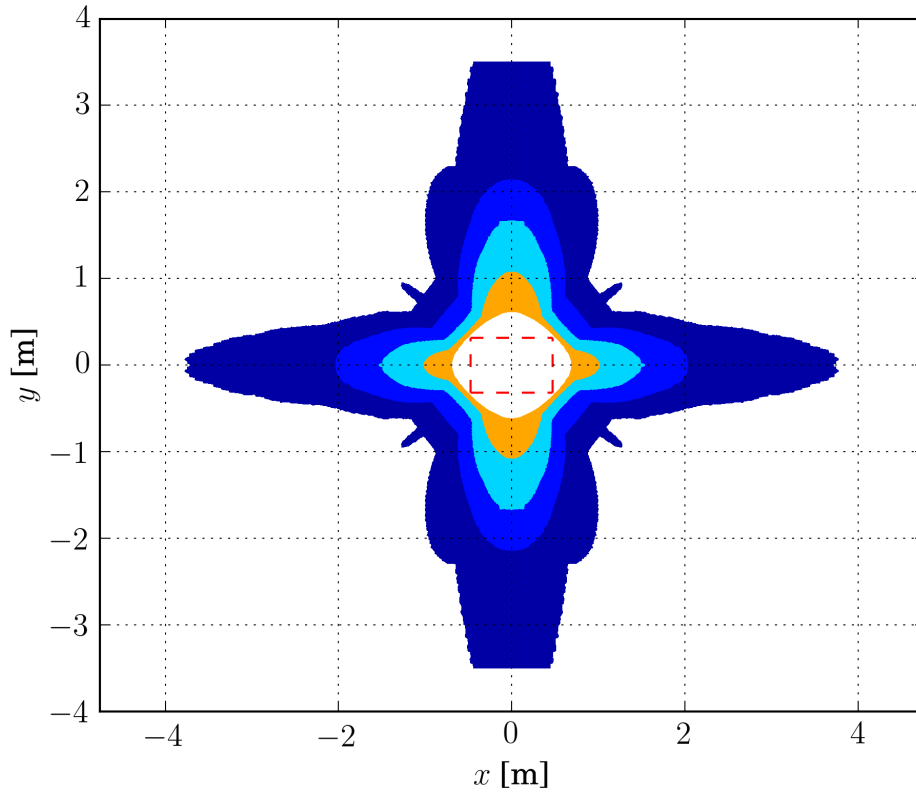


Figure 8: Contours in the  $xy$ -plane of the case-maximum of  $p_{\max}(x, y)$  for cases M1–M3 and their reflections. Contour levels increase by a factor two for each band and equal  $0.2 < p_{\max} < 0.4$  (dark blue),  $0.4 < p_{\max} < 0.8$  (blue),  $0.8 < p_{\max} < 1.6$  (turquoise) and  $1.6 < p_{\max} < 3.2$  (orange). The edges of the dynamite stack (real dimensions) are marked by red, dashed lines.

The contours in the figure are symmetric around the  $x$ - and  $y$ -axes, since plane initiations from all sides of the stack are included in the case-maximum. As seen earlier (in Figures 6 and 7), there are obvious corner effects in the pressure contours. The pressure quickly drops with distance, from more than 3 kbar (just outside of the stack) to less than 0.2 kbar (at around 3.5 m or less from the sides of the stack), consistent with previously shown data.

### 3.2.4 Discussion: Safety distances

The rationale for defining  $p_{\max}$  as a maximum up to stack height is as follows. Assuming a detonating stack in a storage of multiple stacks of equal height, it is only the pressure values occurring up to stack height that pose a risk to surrounding stacks. Potentially higher pressures above the level of the stack height is irrelevant. The definition of Equation (12) thus allows for the easy estimation of safety distances for storing multiple stacks alongside each other

If the sensitivity of a given explosive is known (e.g. based on gap-tests in air), it is thus trivial to estimate required safety distances based directly on the results of the previous section. Assuming the sensitivity of a hypothetical explosive to be, say, 0.4 kbar, a circular safety distance of 2.2 m can be determined based on Figure 8.

More useful information can also be extracted with regards to safety distances: It is clear from Figure 8 that the required safety distance is much larger in the directions perpendicularly from the sides of the stack than diagonally from the side edges. In the latter case, the required safety distance for the hypothetical explosive is merely 0.7 m. Hence, a staggered arrangement of stacks will allow for more compact storage without increasing the risk of sympathetic detonation.

Moreover, the simulation methodology presented in the above enables further testing of case-specific storage, such as effects of shock reflections from ceilings (for indoor storage), or quantitative investigations of clustered storage, in which several stacks are stored close together (allowing for a limited stack-to-stack propagation), but with correspondingly larger distances between stack clusters.

Note, however, that the pressure sensitivity of an explosive – if known – only constitutes one risk factor. Sensitivity to mechanical impacts, specifically from any solid fragments from nearby explosions, represents another real and considerable risk which has not been considered in the foregoing discussion.

## 4 Concluding remarks

A novel two-step approach to simulating detonations of explosives has been demonstrated, combining thermochemical calculations with gas-dynamical computations. The methodology allows for the simulated detonation of several different explosives and charge geometries, as well as subsequent shock interaction with surrounding structures, in up to three spatial dimensions.

The simulation methodology has been validated against earlier experimental and numerical work on TNT detonations. New TNT equivalencies have been computed for a selection of common commercial explosives.

Data has also been presented on simulated detonations of a stack of dynamite, using a variety of initiation locations, and resulting pressure fields and implied safety distances have been discussed.

For a detonating stack of dynamite, plane initiations of the detonation generally yields the highest pressure levels. Furthermore, the pressures are significantly higher in the directions perpendicularly from the sides of the stack compared to the directions diagonally from the side edges of the stack. As expected, the pressure levels drop quickly with distance, from more than 3 kbar (just outside of the stack) to less than 0.2 kbar (at around 3.5 m or less from the sides of the stack).

The simulations and data processing demonstrated here can be easily used to determine required safety distances for storage of an explosive, given that empirical data on the pressure sensitivity of the explosive is available.

## Appendix

### A An indication of the mesh-resolution sensitivity

At this time, no rigorous study of the mesh-resolution sensitivity of the results has been carried out. Moreover, the effect of using first-order face-value reconstruction instead of the ENO scheme has not been evaluated, since this scheme was not stable for the three-dimensional simulations. These investigations will be included in future work.

That said, the comparison between case K2 (on a 26 million-cell mesh) and case L3 (on a 47 million-cell mesh) gives an important indication of the significance of the mesh resolution; as shown in Figure 9, the difference in pressure levels appear to be insignificant when comparing the high-resolution case to the low-resolution case.

More extensive studies should be carried out to ensure that also the *gradients* of pressure and density are well represented by the present choice of parameters. Furthermore, the differences might be more significant at higher pressure levels, such as if plane initiations or detonations of larger amounts of explosive were to be compared.

For now, however, it is tempting to conclude that the present choice of mesh resolution seems quite sufficient for the results which are the focus of this paper.

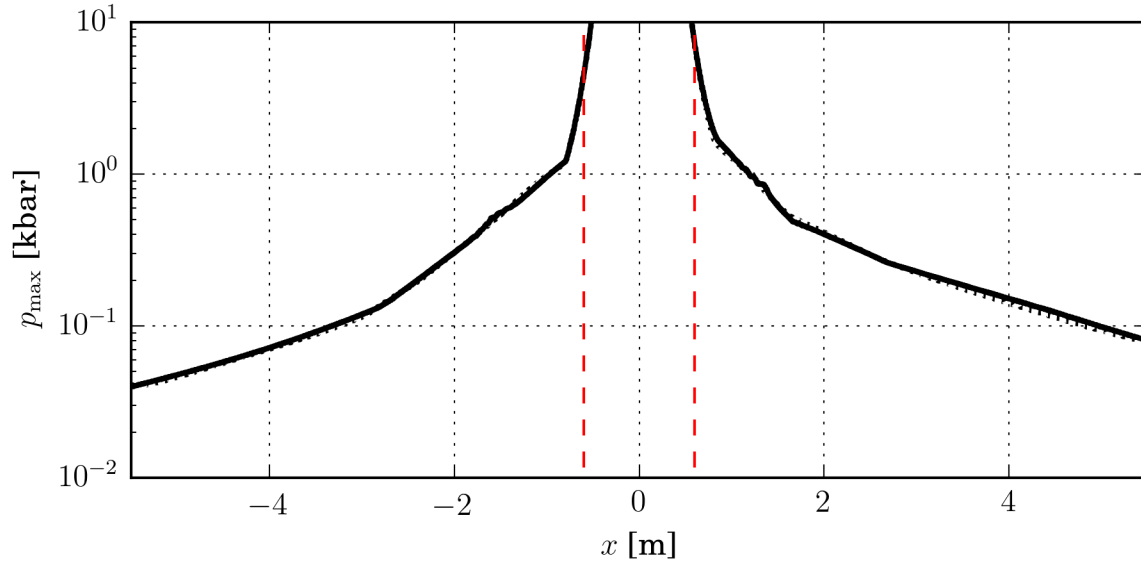


Figure 9: Maximum pressure,  $p_{\max}$ , as a function of  $x$ -distance (with  $y = 0$ ) from the center of the dynamite stack for cases K2 (—), and L3 (·····). The edges of the dynamite stack (real dimensions) are marked by vertical, red (dashed) lines.

## References

- [1] R. Jeremić and Z. Bajić, “An approach to determining the TNT equivalent of high explosives,” *Sci. Tech. Rev.*, vol. 56, no. 1, pp. 58–62, 2006.
- [2] R. Panowicz, M. Konarzewski, M. Trypolin, R. Panowicz, and M. K.-M. Trypolin, “Analysis of criteria for determining a TNT equivalent,” *Strojniški vestnik-Journal of Mechanical Engineering*, vol. 63, no. 11, pp. 666–672, 2017.
- [3] M. Sućeska, “Calculation of detonation parameters by EXPLO5 computer program,” in *Explosion, Shock Wave and Hypervelocity Phenomena in Materials*, vol. 465 of *Materials Science Forum*, pp. 325–330, Trans Tech Publications, 8 2004.
- [4] M. Sućeska, “EXPLO5 Version 6.02/2014 User’s Guide,” *OZM Research*, 2014.
- [5] G. Bres, Y. Khalighi, F. Ham, and S. Lele, “Unstructured large-eddy simulation technology for aeroacoustics of complex jet flows,” in *40th International Congress and Exposition on Noise Control Engineering (Inter-Noise 2011), Osaka, Japan, Sept*, pp. 4–7, 2011.
- [6] Cascade Technologies Inc., *User’s and Developer’s Manual; Jefferson Release Version 4.1.0*, February 2014.

- [7] G. Dantzig, S. Johnson, and W. White, “A linear-programming approach to the chemical equilibrium problem,” *Management Science*, vol. 5, no. 1, pp. 38–43, 1958.
- [8] S. Gryś and W. A. Trzciński, “Thermodynamic modelling of processes of combustion, explosion, and detonation of non-ideal high energetic systems (in Polish),” *Biuletyn Wojskowej Akademii Technicznej*, vol. 59, no. 3, pp. 71–118, 2010.
- [9] G. Allaire, S. Clerc, and S. Kokh, “A five-equation model for the simulation of interfaces between compressible fluids,” *Journal of Computational Physics*, vol. 181, pp. 577–616, Sep 2002.
- [10] E. F. Toro, M. Spruce, and W. Speares, “Restoration of the contact surface in the HLL-Riemann solver,” *Shock waves*, vol. 4, no. 1, pp. 25–34, 1994.
- [11] J. H. S. Lee, *The Detonation Phenomenon*. Cambridge University Press, 2008.
- [12] A. Kuhl, “On the structure of self-similar detonation waves in TNT charges,” *Combustion, Explosion, and Shock Waves*, vol. 51, no. 1, pp. 72–79, 2015.
- [13] J. Bdzil, D. S. Stewart, and T. L. Jackson, “Program-burn algorithms based on detonation shock dynamics: discrete approximations of detonation flows with discontinuous front models,” *Journal of Computational Physics*, vol. 174, no. 2, pp. 870–902, 2001.
- [14] A. Kapila, J. B. Bdzil, and D. S. Stewart, “On the structure and accuracy of programmed burn,” *Combustion Theory and Modelling*, vol. 10, no. 2, pp. 289–321, 2006.
- [15] H. Y. Grisaro and I. E. Edri, “Numerical investigation of explosive bare charge equivalent weight,” *International Journal of Protective Structures*, vol. 8, no. 2, pp. 199–220, 2017.
- [16] C. N. Kingery and G. Bulmash, *Airblast parameters from TNT spherical air burst and hemispherical surface burst*. US Army Armament and Development Center, Ballistic Research Laboratory, 1984.